Canadian Science Publishing | Canadian Journal of Civil Engineering

Influence of Web Geometry on Concrete Masonry Walls Subject to Out-of-Plane Loading

Journal:	*Canadian Journal of Civil Engineering*
Manuscript ID	cjce-2024-0259.R1
Manuscript Type:	Research Article
Date Submitted by the Author:	28-Nov-2024
Complete List of Authors:	Heide, Micah; Atkinson-Noland & Associates Feldman, Lisa R.; lisa.feldman@usask.ca, Department of Civil and Geological Engineering; University of Saskatchewan,
Is the manuscript for consideration in a Special Issue or Collection?:	Not applicable (regular submission)
Keyword:	concrete masonry unit geometry, flexural response, flexural stiffness, partially grouted and reinforced masonry walls, out-of-plane behavior

INFLUENCE OF WEB GEOMETRY ON CONCRETE MASONRY WALLS SUBJECT TO OUT-OF-PLANE LOADING

BY:
Micah Heide,[a] Engineer Intern
Lisa R. Feldman,[1, b] Professor & Head

[a]Atkinson-Noland & Associates
2619 Spruce St.
Boulder, CO, USA 80302

[b]Department of Civil, Geological, and Environmental Engineering
57 Campus Drive
Saskatoon, SK, Canada S7N 5A9

[1]Corresponding Author

Word Count = 9097 equivalents

ABSTRACT

An experimental program consisting of 27 partially grouted and reinforced walls was conducted to assess the impact of concrete masonry unit (CMU) web geometry on flexural response when subject to out-of-plane loading given changes to CMU geometry as adopted by ASTM C90 in 2011 that have yet to be vetted in Canada. All walls had the same overall geometry and were constructed with either regular stretcher units conforming to either CSA A165-14 or ASTM C90-23 or knock-out units conforming to ASTM C90-23. The configuration of the longitudinal reinforcement was also varied between wall series such one of that three reinforcing ratios resulted: 0.22, 0.44, or 0.66%. No notable differences in behavior resulted due to differences in the geometry of the concrete masonry units used in wall construction, though the grout columns as included in the reinforced cells appeared to mask the influence of web geometry.

Keywords: concrete masonry unit geometry, flexural response, flexural stiffness, partially grouted and reinforced masonry walls, moment-curvature analysis, out-of-plane behavior

1. INTRODUCTION

Prior to 2011, the geometry of concrete masonry units (CMUs) produced in the United States and Canada were identical. However, the 2011 edition of ASTM C90 (2011) included changes to CMU geometry to better meet new energy efficiency requirements as were adopted by various states. Web thickness was reduced to a minimum of 19 mm for all CMU sizes, and the concept of a normalized web area, A_{wn}, was introduced and calculated as:

$$A_{wn} = \frac{T_w H_w N_w}{L_n H_n} \leq 45{,}140 \text{ mm}^2/\text{m}^2 \quad [1]$$

where T_w is the web thickness (in mm), H_w is the web height (mm), N_w is the number of webs included in the CMU, L_n is the nominal CMU length (m), and H_n is the nominal height of the CMU (i.e. that of the face shells). Up to a 30% increase in thermal resistance is expected depending on the geometry of the partially grouted and reinforced wall system considered (Lang & Thompson 2014). In contrast, CMU geometry as included in the most recent edition of CSA A165 (2014a), remains unchanged from the original edition as was published in 1977 (CSA 1977) and included web thicknesses that varied from 20 to 30 mm as nominal CMU size increased from 200 to 300 mm. The minimum height of knock-out webs, as is a function of the normalized web area in ASTM C90 (2023), is unspecified in CSA A165 (2014a) but is typically provided as 120 mm by Canadian block producers.

Changes to web geometry as included in ASTM C90 (2011) and more recent editions of this standard have many benefits in addition to the increased thermal resistance of masonry assemblages as previously noted. The reduced weight of CMUs allows for more economical transportation and so can benefit isolated and indigenous communities, reduces construction timelines, and potentially reduces the likelihood of workplace injuries to masons. The latter is of

particular significance given that the Workplace Safety and Insurance Board of Ontario (2018) reported that the masonry rate cost per insurance claim is 2.44 times that of all other construction class rate groups. Further, differences in CMU geometry as used in Canada and the United States impedes the ability to exchange products and knowledge across our common border and stands to disadvantage Canada disproportionally due to our smaller population and thus masonry industry.

Chhetri and Feldman (2023) conducted an experimental program consisting of 126 one CMU wide by 3 course tall grouted or hollow masonry prisms constructed in running bond with face shell bedding. Prisms were either constructed with regular stretcher units conforming to the geometric requirements included in CSA A165 (2014a), or knock-out units conforming to either CSA A165 (2014a) or ASTM C90 (2023). The as-tested strength of grouted prisms was determined to be independent of CMU size or web height whereas statistically significant differences in as-tested strengths were reported for hollow prisms constructed using knock-out CMUs conforming to ASTM C90 (2023) in comparison to those constructed using either regular stretcher units or knock-out units conforming to CSA A165 (2014a). Savkina and Feldman (2022) then tested 96 one CMU wide by 5 course tall hollow prisms constructed in running bond with face shell bedding subject to either axially concentric or eccentric loading. Prisms were constructed with regular stretcher units meeting the requirements of either CSA A165 (2014a) or ASTM C90 (2023), or knock-out units meeting the requirements of ATM C90 (2023). Little difference in the as-tested capacity was reported when prisms were subject to eccentric loading regardless of the CMU type used in their construction. In contrast, CMU type did influence the as-tested prism strength when axially concentric loading was applied. In such cases, prisms

constructed using regular stretcher units with web geometries conforming to CSA A165 (2014a) requirements had higher capacities than those constructed using regular stretcher or knock-out units conforming to ASTM C90 (2023) requirements.

Webs in CMUs are known to transfer shear between face shells (Lang & Thompson 2014) though only a single analytical investigation was identified (Nasiri & Liu 2019) which investigated this phenomenon. Nasiri and Liu (2019) reported that using CMUs with reduced web thicknesses in unreinforced and ungrouted walls reduced the out-of-plane loading resistance when subject to out-of-plane loading. However, typical construction practice generally requires walls subject to flexure to be partially grouted and reinforced. Such large-scale experimental work that better represents masonry assemblages in practice will bolster the existing test database (Chhetri & Feldman 2023, Savkina & Feldman 2022, Nasiri & Liu 2019) related to the influence of web geometry on member resistance and is presented herein.

2. EXPERIMENTAL PROGRAM

Three parameters were identified that potentially influence the resistance of walls subject to out-of-plane loading: CMU geometry, the longitudinal reinforcement ratio, and the spacing of the longitudinal reinforcement. Table 1 therefore shows that the experimental investigation included a total of nine unique wall configurations, with three replicates of each, for a total of 27 walls. Identification of the walls reported in Table 1 is of the form *TTT-hh-dd*/*SSS* where *TTT* indicates whether CMU geometry meets the requirements of either CSA S304 (CSA 2014b) (CAD) or ASTM C90 (ASTM 2023) (USA), *hh* indicates whether CMU webs are full height (FH) or knock-out (KO), *dd* is the nominal diameter of the reinforcing bars in millimeters, and *SSS* is the centre-to-centre spacing of the longitudinal reinforcing bars in millimeters. Including

three replicates in each test series allowed for the calculation of mean values of resulting test data and for the identification of physical outliers.

Figure 1 shows the overall geometry of all walls included in the experimental program. All walls were 13 courses tall by 2-$1/2$ blocks wide (Fig. 1(a)), were constructed in running bond with face shell mortar bedding, and were partially grouted and longitudinally reinforced (Figs. 1(b) & (c)). The wall width was selected to allow for two unique longitudinal reinforcement layouts (i.e. centre-to-centre spacings of 400 and 800 mm between bars) in conjunction with consistently incorporating a longitudinal bar in the two outmost cells to allow for similar boundary conditions for all walls. The 13-course wall height was chosen to ensure a ductile, flexural failure and so eliminate the need for horizontal (i.e. shear) reinforcement and to provide sufficient development length for all longitudinal reinforcing bar sizes incorporated into the experimental design.

Each wall was constructed with one of three types of CMU geometries to evaluate the influence of this parameter on flexural resistance: regular stretcher units conforming to the geometric requirements of either CSA A165 (CSA 2014a) or ASTM C90 (ASTM 2023), or knock-out units meeting the requirements of ASTM C90 (ASTM 2023). The knock-out units were cut from regular stretcher units conforming to ASTM C90 (ASTM 2023), and so had a web width of 19 mm. The remaining web height of 65 mm used for the knock-out units resulted in a normalized web area, A_{nw}, of 46,313 mm^2/m^2 and so slightly greater than the minimum allowable value of 45,140 mm^2/m^2 provided in ASTM C90 (ASTM 2023). Details of CMU geometries are reported elsewhere (Heide & Feldman 2023).

The spacing of the longitudinal reinforcement dictated the number and placement of grouted cells within the wall's cross-section with the likelihood of web shear failure increasing with increased spacing. Figures 1(b) and (c) show that two spacings of 800 and 400mm, respectively, were therefore incorporated into the experimental design given the constraints provided by the 2-½ CMU wide wall width. Figures 1(b) and (c) show that the outermost wall cells were reinforced in all cases. Figure 1(c) further shows that the middle cell was also grouted and reinforced when the spacing was set as 400 mm.

Walls were also constructed with one of three reinforcement ratios, ρ, as was achieved by varying the size and spacing of the reinforcing bars simultaneously. The resulting three reinforcement ratios were nominally equal to 0.22, 0.44, and 0.66% and fell between the minimum and maximum values for reinforcement in flexural members as prescribed by Clauses 11.2.3.1 and 11.2.2 in CSA S304-14 (CSA 2014b), respectively. Table 1 shows that two combined arrangements of reinforcing bar size and spacing were used to attain the highest of the three selected reinforcement ratios: 15M bars at a spacing of 400 mm on centre (ρ = 0.63%), and 20M bars at a spacing of 800 mm on centre (ρ = 0.66%). The resulting reinforcement ratios were considered to be reasonably equivalent for the purposes of the subsequent analysis.

Table 1 shows that only a single test series included walls constructed with the knock-out CMUs. The size of the reinforcing bars and their centre-to-centre spacing were therefore chosen to result in the midrange reinforcing ratio of 0.44%. Walls in this test series did however include full height webs bordering the grouted and reinforced cells.

2.1 Construction Materials

Two-hundred-millimeter nominal regular stretcher units meeting the requirements of either CSA A165 (CSA 2014a) or ASTM C90 (ASTM 2023) were sourced with all blocks of a given type originating from the same material batch. Web widths for CMUs meeting the geometric requirements of CSA A165 (CSA 2014a) and ASTM C90 (ASTM 2023) were 26 and 19 mm, respectively, and all CMUs were ordered with a specified strength of 15 MPa. Half CMUs and knock-out units were cut in the laboratory to ensure consistency in the mechanical properties for all CMUs with a given web width.

Type S job-prepared mortar with a specified compressive strength of 8.5 MPa was mixed in the laboratory. Mix proportions used in mortar batching were consistent with those specified in Table 4 of CSA A179 (CSA 2014c) and included a 1:3 ratio by volume of cement-to-aggregate, and a water-to-cement ratio by volume of 0.7:1.0. Masonry sand with a maximum aggregate size of 5 mm was procured from the Lafarge Aggregates Floral pit and met the requirements for fine aggregate based upon the results of a sieve test conducted in accordance with CSA A23.2-2A (CSA 2014d) requirements. Twenty-three batches of mortar were included in the investigation with 6 cubes cast and tested from each. A resulting mean mortar cube strength of 10.4 MPa (COV = 21.7%) resulted (Heide 2023).

Standard high slump grout was mixed in the laboratory with a target slump range of 200 to 250 mm and a minimum specified compressive strength of 12.5 MPa as per the requirements of CSA A179 (CSA 2014c). The grout was batched with cement-to-aggregate and water-to-cement ratios of 1:5 and 1:1 by volume, respectively. Pre-blended fine and coarse aggregate with a

maximum aggregate size of 14 mm met the gradation requirements included in CSA A179 (2014c) based upon the results of a sieve analysis. Mean strengths of 8.90 MPa (COV = 21.5%) and 12.2 MPa (COV = 19.7%) resulted for the non-absorbent grout cylinders and absorbent grout prisms, respectively.

Grade 400 steel reinforcement with nominal diameters of 10, 15, and 20 mm meeting the requirements of G30.18-21 (CSA 2021) were procured in 6 m lengths. All bars of a given size originated from a single heat lot. Three intact lengths of each size of reinforcing bars included in the experimental program were tested in accordance with procedures described in ASTM A370 (ASTM 2022). Table 2 reports the mean values of the resulting mechanical properties obtained for each bar size.

2.2 Construction

Table 1 shows that walls were constructed and tested in two phase given space constraints in the laboratory. Walls longitudinally reinforced with 10M or 20M bars were included in the first construction phase whereas the second phase included all walls longitudinally reinforced with 15M bars. Addition details related to the construction process are included elsewhere (Heide 2023).

Twenty-five-millimeter-thick steel base plates, elevated above the lab floor by setting them atop CMUs at each end, served as a platform upon which to construct each wall. The walls were constructed in two CMU lifts: a first of 7 courses and a subsequent 6 course lift. The longitudinal reinforcing bars were placed in the intended cells following the first CMU lift followed by grout placement to a height of 6.5 courses. This first grout lift intentionally

terminated 0.5 courses below the top of the partially constructed wall to eliminate a plane of weakness at the level of the mortar joint between the 7th and 8th block courses. Grout was left to cure overnight prior to the construction of the second, 6 course tall CMU lift which required threading the CMUs over the reinforcing bars that were already in place. The final 6.5 course tall grout lift then followed.

Care was taken to ensure the proper alignment of the reinforcing bars along the wall height and followed methods used by others (e.g. Sanchez and Feldman 2015, Kisin and Feldman, 2015, Kelln and Feldman 2015). Holes that were sufficiently large to accommodate the bars were pre-drilled in the steel base plates to ensure their proper positioning at the bottom of the wall. Strips of welded wire mesh were then placed within the mortar joints above the 4th and 10th block courses, and so allowed the reinforcing bars to be threaded through them to further ensure their vertical alignment along the wall height.

Twenty-seven grouted and 15 ungrouted one CMU wide by three course tall prisms were constructed in running bond using face shell mortar bedding and tested in accordance with Annex D in CSA S304-14 (CSA 2014b). One grouted prism was constructed corresponding to each wall included in the experimental design, and three ungrouted prisms were constructed for each combined CMU type and web height included for walls constructed and tested in each construction phase. Grouted prisms were tested on the same day as the corresponding wall. Ungrouted prisms testing was spread out within each construction phase such that a prism was tested within one day of each wall test it was intended to represent. Mean compressive strengths

of 10.5 MPa (COV = 9.61%) and 19.5 MPa (COV = 12.1%) resulted for the grouted and ungrouted prisms, respectively.

Table 1 shows the resulting prism strengths corresponding to each wall included in the test program. As-tested strengths were reported directly for the ungrouted prisms while results reported for grouted prisms were adjusted by multiplying their as-tested resistance by the 0.9 correction factor for prisms with a height-to-thickness ratio of three as required by Table D.1 in CSA S304-14 (CSA 2014b).

2.3 Instrumentation and Testing

Walls were subject to four-point loading and tested 28 to 36 days following their construction. Described herein are a description of the test setup including details relating to their top and bottom supports, and the instrumentation used during testing of each wall.

Figures 2 and 3(a) show a schematic and photograph, respectively, of the overall test setup, and Figures 3(b) and (c) show details of the bottom and top support assemblies with additional details provided elsewhere (Heide 2023). Figure 2 shows that the walls were tested using a single actuator with a capacity of 250 kN in displacement control at a rate of 6 mm/min. A spreader beam system was used to apply load to each wall at mid-height of the 5th and 9th CMU courses, and so 400 mm above and below mid-height of the wall. Horizontal spreader beams were used to distribute the loads uniformly across its width. Load cells, with capacities of 250 kN, were located between the horizontal spreader beams dictating the location of the top and bottom load points and the wall to allow the magnitude of the applied loads to be captured during

testing. Figure 2 further shows that the top and bottom shear span lengths, including for the height of the top and bottom support assemblies, were 965 and 923 mm, respectively.

Figure 3(b) shows that a grooved steel plate was bolted to the underside of the steel base plate that supported each wall. The groove in this plate received the 1600x400x7 (length x height x thickness in millimeters) vertically oriented plate that served as a knife edge and so allowed for a pinned support condition at the base of the wall (i.e. such that rotation was permitted but horizontal and vertical displacements were prevented). Steel angles (L102x102x13) were bolted to the steel base plate with a thin layer of plaster applied between the vertical leg of the angle and either the front or back wall face to ensure uniform contact.

Figure 3(c) shows that a 1000x458x25 (length x width x thickness in millimeters) slotted steel plate was placed atop the wall once it has been moved into the test bed with the bottom support established. As per the bottom support, two L102x102x13 steel angles adjacent to the front and back wall faces were bolted to the slotted steel plate. A thin layer of plaster placed between the vertical legs of the angles and the wall face ensured uniform contact. These angles prevented out-of-plane displacement at the top of the wall. Three 16 mm diameter steel braces then connected the slotted steel plate to the test frame with ball joints located at each end. Such an assembly simulated an ideal vertical roller support that allowed for rotation and vertical displacement but prevented horizontal displacement at the top of the wall.

Figure 2 shows that four laser displacement gauges were rigidly connected to an independent rolling frame and therefore not subject to deformations incurred by the test frame. This rolling

frame was moved away from the wall following testing and put back into place once the subsequent wall was set up for testing. Two of the laser displacement gauges had a range of 750 mm and were located 200 mm above and below mid-height of the wall (i.e. at mid-height of the 3rd and 7th CMU courses) and the other two gauges had a range of 100 mm and were located 800mm above and below the wall mid-height (i.e. at mid-height of the 3rd and 11th CMU courses). All four gauges were located at the wall centreline. A fifth and final laser displacement gauge with a range of 100 mm was used to measure the horizontal displacement of the slotted steel plate located at the top of the wall.

Data from the load cells and laser displacement gauges were collected at a rate of 1 Hz during wall testing. Two high-speed cameras were also used to capture images of the tensile face of each wall at a rate of 0.1 Hz as testing progressed and were used to analyze the crack patterns that developed.

3. TEST RESULTS AND ANALYSIS

Table 1 shows the as-tested prism strength, deflections, and the total loads recorded by the upper and lower actuators combined at crack initiation, first yielding of the longitudinal reinforcement, and the maximum load level. The following discussion addresses visual observations made during testing, bending moment resistances and calculated midspan deflections, and wall behavior as predicted from a moment-curvature analysis.

3.1 Visual Observations

Walls were assumed to be uncracked prior to testing, with cameras set up to monitor cracking on the tension face as testing progressed. The visual range of the cameras was from midspan of the 4th to 10th CMU courses. The mortar joints that were out of range of the cameras were visually

inspected for cracks following testing. Figures showing the failure modes of the walls are included elsewhere (Heide 2023).

Cracking typically initiated in the mortar joints within the constant moment region between the two points of applied load and so in the mortar joints located between the 5th and 6th, and 8th and 9th CMU courses. These cracks widened as testing progressed. Cracking then appeared in the mortar joints within the shear spans, and minor hairline cracks were identified following testing in the mortar joints outside of the range of the cameras. This crack pattern matched that anticipated for all walls based upon the loading and support conditions irrespective of the CMU type used in their construction.

The extent of spalling on the compression face of each wall, as examined visually following testing, increased with increasing reinforcement ratio. The bending moment, and hence compressive force, that resulted increased with increasing reinforcement ratio whereas the mechanical properties of the cementitious materials used in all walls were similar. The severity of spalling further appeared similar for walls with any given reinforcement ratio irrespective of the geometry of the CMUs used in their construction.

Two walls (IDs CAN-FH-20/800-1 and CAN-FH-20/800-2) failed atypically due to debonding of the mortar in the bed joint between CMUs in the 12th and 13th courses from the bottom of the wall. Workmanship problems including inadequate tapping of CMUs and extended curing of the mortar prior to placing CMUs in the 13th course appeared to be the source of these failures. A review of the load versus displacement behavior for these walls showed that their failures

occurred following yielding of the reinforcing steel but prior to attainment of the maximum load achieved as a result of a flexural failure. Test data collected for these walls at the maximum load level were therefore deemed to be physical outliers.

3.2 Bending Moment Resistance and Calculated Midspan Deflection

Table 1 shows the total loads recorded by the two load cells combined at first cracking, yielding of the reinforcement, and the maximum load level. First cracking and yielding of the reinforcement were defined by the sudden changes in slope in the load-displacement response for each wall. The maximum load level represents the peak total load (i.e. the sum of loads recorded simultaneously by the upper and lower load cells). Loads recorded by the upper and lower load cells were not identical (Heide 2023). Rather, loads recorded by the load cell placed at the vertical level of the lower spreader beam were typically higher than those recorded at the level of the upper spreader beam. The hinge on the hydraulic actuator (Figs. 2 and 3(a)) allowed the vertical spreader beam to rotate. Figure 2 further shows that the length of the shear span at the bottom of the wall is slightly shorter than that located at the top of the wall and so resulted in higher loads recorded by the lower load cell in comparison to those recorded by the upper load cell.

Figures 4(a) and (b) show the as-tested moments at yielding of the reinforcing steel and the maximum load level, respectively. As-tested moments were calculated from statics based upon the four-point loading arrangement shown in Figure 2 and total loads reported in Table 1 from the upper and lower load cells. The as-tested moments at the maximum load level for CAD-FH-20/8000 and CAD-FH-20/800-2 were excluded from Figure 4(b) as they were identified as physical outliers. A mean difference of 1.53% was noted between the as-calculated moments

and those obtained assuming equal distribution of loading between the two application points and so was deemed negligible. Figures 4(a) and (b) show that, for any given longitudinal reinforcing bar arrangement, as-tested moments are insensitive to the CMU geometry used in wall construction at both yielding of the reinforcing steel and the maximum load level.

Figure 5 shows the ratio of as-tested to CSA S304-14 (CSA 2014a) predicted values of bending moment resistance at the maximum load level. Predicted values of the moment were calculated by setting the partial material resistance factors for the masonry assemblage and reinforcing steel strengths to unity and using the as-tested values of prism strength and steel yield strength as are reported in Tables 1 and 2, respectively. Figure 5 shows that the ratio of the as-tested maximum moment to that predicted using the provisions included in CSA S304-14 (CSA 2014a) exceeded 1.0 for all walls and ranged from 1.01 to 1.13. These results suggest that the calculation method for flexural resistance as included in CSA S304-14 (CSA 2014a) are reasonable and conservative for members constructed with CMUs meeting the geometric requirements of either CSA S304-14 (CSA 2014b) or ASTM C90-23 (ASTM 2023).

Figure 6 shows a schematic of deflections along the wall height. A non-zero horizontal deflection, δ_{sp}, was invariably measured for all walls by the laser displacement gauge located at the height of the slotted plate used in the top support assembly. This resulted in the addition of linearly distributed displacements over the wall height (i.e. the area between the vertical line at the left-hand side of Figure 6(b) and the angled dashed line) varying from zero at the bottom support to δ_{sp} at the top support to the otherwise assumed parabolic distribution resulting from

the four-point loading arrangement. The total as-measured displacement of the laser displacement gauges located along the height of the wall, δ_i, was then equal to:

$$\delta_i = \delta_{i,w} - \delta_{i,sp} \quad [2]$$

where $\delta_{i,w}$ is the anticipated displacement at the i^{th} strain gauge located along the wall height resulting from the four-point loading arrangement and $\delta_{i,sp}$ is the linear correction resulting from the horizontal movement of the slotted plate included in the top support assembly as calculated by:

$$\delta_{i,sp} = \frac{h_i}{l} \cdot \delta_{sp} \quad [3]$$

where h_i is the distance between the i^{th} laser displacement gauge and the centreline of the bottom support and l is the wall span.

None of the laser displacement gauges were located at mid-height of the wall and so did not capture the approximate maximum displacement. Instead, displacement along the wall was approximated theoretically using the double integration method based upon the moment distribution along the wall height. Table 1 reports these values at loads corresponding to first cracking, yielding of the reinforcement, and the maximum load level. Good agreement was achieved when compared to corrected displacements measured at the location of the laser displacement gauges, $\delta_{i,w}$, and the deflected profile as theoretically obtained. Differences were typically attributed to the rigid body motion typical of reinforced masonry construction (i.e. with cracking typically confined to bed joints). No differences were noted for walls constructed using different CMU geometries.

3.3 Wall Behavior as Predicted using a Moment-Curvature Analysis

A moment-curvature analysis was conducted to theoretically predict the bending moment and deflection expected of the walls as included in the experimental investigation and was similar to that reported by others (e.g. Ahmed & Feldman 2012, Kisin & Feldman 2015, Vachon & Feldman 2023). A modified Park-Kent curve (Priestley & Elder 1983) was used to model the stress versus strain behavior of the masonry in both the grouted and ungrouted regions of the wall and was based on the as-tested masonry strengths obtained from prism testing reported in Table 1. A weighted average based upon cross-sectional areas associated with grouted and ungrouted regions of each wall was used to establish the effective assemblage strength. The stress versus strain behavior of the longitudinal reinforcing steel was based on the mechanical properties of as-tested lengths of these bars as reported in Table 2 assuming a three-stage model: (1) a linear-elastic region, (2) a yield plateau, and (3) a strain hardening region represented by a cubic function.

A linear and proportional moment-curvature response was assumed prior to cracking. Following cracking, the moment-curvature response was established iteratively: the depth to the neutral axis was varied until a 0.5% difference or less was achieved between the tensile force in the reinforcement and the compressive force in the cementitious materials to achieve force equilibrium. Strain compatibility was further assumed between the reinforcing steel and the surrounding cementitious materials.

The moment-curvature response was established assuming that load was distributed equally to the two horizontal spreader beams. The midspan deflection was then calculated as the summation of lateral deflections of a finite number of wall segments at any given load level. A

sensitivity analysis of select walls (IDs: CAD-FH-10/800-1, CAD-FH-15/800-1, CAD-FH-20/800-1, and CAD-FH-14/400-1) were conducted for four levels of applied load (15, 20, 40, and 45 kN) and showed that convergence was established when the wall was divided into 100 segments.

The moment-curvature analysis was conducted with consideration to the different requirements for the effective compressive width as included in CSA S304-14 (2014b) and TMS402/602-22 (2022). Clause 10.6.1 in CSA-S304-14 (2014b) requires the effective compressive width to be the lesser of the centre-to-centre spacing between the longitudinal reinforcing bars and four times the wall thickness. Clause 5.1.2.1 in TMS402/602-22 (2022) alternatively requires the effective compressive width to be the lesser of: (1) the centre-to-centre spacing of the longitudinal reinforcing bars, (2) six times the nominal wall thickness, and (3) 1830 mm (72 in.). No difference in the effective compressive width resulted for walls where the centre-to-centre spacing between longitudinal bars was 400 mm. In contrast, the effective compressive width of walls with centre-to-centre spacing between longitudinal reinforcing bars of 800 mm was 760 and 800 mm when calculated in accordance with provisions included in CSA S304-14 (2014b) and TMS402/602-22 (2022), respectively. Results for walls with an 800 mm centre-to-centre spacing between longitudinal reinforcing bars showed that theoretically predicted values of the moment at midspan were 7.97 and 7.62% greater than those derived from the test data when calculated using provisions for the effective width of the compression zone as are included in CSA S304-14 (2014b) and TMS 402/602-22 (2022), respectively. In contrast, a mean error of 10.1% in flexural stiffness was calculated using provisions for the effective width of the compression zone as included in CSA S304-14 (2014) and so was slightly less than the 10.7%

399 resulting when provisions as included in TMS 402/602-22 (2022) were implemented in the
400 moment-curvature analysis. Results therefore suggest that provisions for the width of the
401 effective compression zone as included in CSA S304-14 (2014b) better predicted the post-
402 cracking flexural stiffness whereas those included in TMS 402/602-22 (2022) better predicted
403 flexural resistance. Provisions for the calculation of the effective width of the compression zone
404 as included in TMS 402/602-22 (2022) were used exclusively moving forward with this analysis
405 given that accuracy related to flexural resistance was considered more important than for flexural
406 stiffness.
407
408 The normalized moment resistance for each wall was calculated as the moment resistance
409 obtained from the test data divided by that theoretically calculated from the moment-curvature
410 analysis and are shown in Figures 7(a) and (b) at yielding of the longitudinal reinforcement and
411 the maximum load level, respectively. Figures 7(a) and (b) both show that variations in both
412 CMU web geometry and configuration of the longitudinal reinforcement generally had no
413 notable effect on the resulting normalized moment resistance. Figure 7(b) does, however, show
414 that resulting normalized moment resistances for walls reinforced with 10M longitudinal bars
415 were less than unity at the maximum load level, and result because strain hardening of the
416 longitudinal reinforcement was assumed for all bar sizes within the moment-curvature analysis.
417 In contrast, strain hardening of the longitudinal reinforcement was not apparent from the load
418 versus deflection results for walls longitudinally reinforced with 10M bars as was obtained from
419 testing.
420

Figure 8 shows the normalized post-cracking flexural stiffness. The theoretical post-cracking flexural stiffness, κ_{th}, was calculated from the moment-curvature analysis as:

$$\kappa_{th} = \frac{P_{y,th} - P_{cr,th}}{\Delta_{y,th} - \Delta_{cr,th}} \quad [4]$$

where $P_{cr,th}$ and $P_{y,th}$ are the theoretically calculated loads corresponding to first cracking and yielding of the longitudinal reinforcing steel, respectively; and $\Delta_{cr,th}$ and $\Delta_{y,th}$ are the theoretically calculated mid-height wall deflections at first cracking and yielding of the longitudinal reinforcing steel, respectively. The post-cracking flexural stiffness influences the load-deflection behavior. Figure 8 shows that the theoretically calculated value of the post-cracking flexural stiffness is generally over-estimated when compared with that calculated from load-deflection data collected during wall testing. Results are similar for wall series with similar configurations of longitudinal reinforcing steel but differing CMU geometry, suggesting that partial cell grouting obscures the effect of web geometry.

4. SUMMARY AND CONCLUSIONS

This paper presents the results of an experimental investigation conducted to examine the influence of concrete masonry unit web geometry on the behavior of partially grouted and longitudinally reinforced walls subject to out-of-plane loading. ASTM C90 was revised in 2011 to modify the geometric requirements of concrete masonry units. These provisions allow for thinner webbed units and/or deeper knockout units than are permitted by CSA A165, thereby reducing transportation costs, construction time, and the likelihood of workplace injuries. This investigation forms part of a larger experimental program and included 27 partially grouted and reinforced walls with three replicates in nine test series. All walls were 13 courses tall and 2-½ blocks wide and were subject to four-point loading with 1560 mm between the two points of applied load. Resulting flexural capacity and behavior was compared when walls were

constructed using one of three longitudinal bar sizes, two bar configurations, and 200 mm concrete masonry units with full height webs conforming to either CSA S165 or ASTM C90 geometric requirements, or knock-out units with geometry conforming to ASTM C90.

Significant conclusions are as follows:

1. Crack patterns that developed during testing matched that expected given the four-point loading arrangement implemented and were similar irrespective of the geometry of the concrete masonry units used in wall construction. The severity of spalling on the wall's compression face was observed to increase with increasing reinforcement.
2. Resulting bending moments occurring at both yielding of the longitudinal reinforcing steel and the maximum load level appeared insensitive to the geometry of the concrete masonry units used in wall construction.
3. The ratio of the as-tested moment occurring at the maximum load level to that predicted using provisions included in CSA S304-14 with partial material resistance factors set to unity and as-tested values of masonry prism and steel yielding strengths ranged from 1.01 to 1.13. These ratios suggest that methods for determining the flexural resistance of masonry walls as are included in CSA S304-14 are reasonable and conservative for members constructed using concrete masonry units conforming to the geometric requirements included in either CSA A165-14 or ASTM C90-22.
4. Deflections as measured by laser displacement gauges were corrected to account for the horizontal displacement that occurred for the slotted plate used in the top support assembly. Nonetheless, these corrected, as-tested displacements correlated well with theoretically predicted deflection profiles obtained from using the double integration

method for the moment distribution imposed over the wall height. No differences were noted for walls regardless of concrete masonry unit geometry.

5. Provisions for the effective width of the compression zone as included in Clause 10.6.1. of CSA S304-14 better predicted the post-cracking flexural stiffness as was calculated using a moment curvature analysis whereas those included in Clause 5.1.2.1 of TMS 402-22 better predicted flexural resistance.
6. Concrete masonry unit geometry and configuration of the longitudinal reinforcement had no notable effect on the ratio of the maximum moment resistance obtained from testing to that calculated theoretically from a moment-curvature analysis at either yielding of the reinforcement or the maximum load level.
7. The theoretically calculated post-cracking flexural stiffness of the walls was generally over-estimated when compared to that obtained from test results and were similar for walls constructed with concrete masonry units with different geometries.

Partial grouting of the walls obscured the influence of concrete masonry unit web geometry on out-of-plane wall behavior. Additional testing is therefore recommended using walls containing unbonded reinforcement anchored at their top and bottom to better evaluate the effect of concrete masonry unit web geometry on shear transfer between face shells. Testing should also be extended to include a broader range of reinforcement ratios and configurations of the reinforcing steel.

ACKNOWLEDGEMENTS

The authors gratefully acknowledge financial support as provided by Mitacs, the Natural Sciences and Engineering Research Council of Canada, the Canada Masonry Centre, and the

Canadian Concrete Masonry Producers Association. In-kind support, in the form of material supply and mason's time, was provided by the Saskatchewan Masonry Institute. The first author also acknowledges scholarship support as provided by the University of Saskatchewan. Thanks are also extended to Monty Norby, City Masonry, for the construction of all specimens, and Brennan Pokoyoway, Structural Lab Technician at the University of Saskatchewan.

Competing interests: The authors declare that there are no competing interests.

Data availability: Data generated and analyzed during this study are available upon request from the corresponding author.

REFERENCES

Ahmed, K. Feldman, L.R. 2012. Evaluation of contact and noncontact lap splices in concrete block masonry construction, Canadian Journal of Civil Engineering, V. 39, No. 5, pp. 515 – 525. Doi: 10.1139/12012-026.

ASTM. 2022. ASTM A370-22 Standard test methods and definitions for mechanical testing of steel products. ASTM International. West Conshohocken, PA.

ASTM. 2023. ASTM C90-23 Standard specification for loadbearing concrete masonry units, ASTM International, West Conshohocken, PA.

ASTM. 2011. ASTM C90-11b – Standard specification for loadbearing concrete masonry units. ASTM International, West Conshohocken, PA.

Chhetri, N., Feldman, L.R. 2023. Impact of concrete masonry unit geometry on masonry assemblage strength, Canadian Journal of Civil Engineering, https://doi.org/101139/cjce-2023-0121.

CSA. 1977. A165SI-1977 Supplement no. 1 to CSA A165 series, standards on concrete masonry units, Canadian Standards Association, Mississauga, ON.

CSA. 2014a. CAN/CSA A165-14 (R2019) – Standard on concrete masonry units. Canadian Standards Association, Rexdale, ON.

CSA. 2014b. CAN/CSA S304-14 (R2019) – Design of masonry structures. Canadian Standards Association, Rexdale, ON.

CSA. 2014c. CAN/CSA A179-14: Concrete masonry units. Canadian Standards Association, Rexdale, ON.

CSA. 2014d. CAN/CSA A23.2-2A-14 Construction materials and concrete construction/test methods and standard practices for concrete. Canadian Standards Association, Mississauga, ON.

CSA. 2021. CAN/CSA G30.18-21 - Carbon steel bars for concrete reinforcement. Canadian Standards Association, Mississauga, ON.

Heide, H., Feldman, L.R. 2023. Influence of web geometry on concrete masonry walls subject to out-of-plane loading. 14th North American Masonry Conference, Omaha, NE.

Heide, M. 2023. Influence of web geometry on concrete masonry walls subject to out-of-plane loading. M.Sc. thesis, University of Saskatchewan, Saskatoon, SK.

Kelln, R.D., Feldman, L.R. 2015. Bar size factors for lap splices in block walls subjected to flexure. Canadian Journal of Civil Engineering, 42(8), pp. 521 – 529.

Kisin, A., Feldman, L.R. 2015. Corrective measures for noncontact splices in concrete block masonry. ACI Structural Journal, 112(4), pp. 475 – 484.

Lang, N.R., Thompson, J.J. 2014. Recent changes to ASTM specification C90 and impact on concrete masonry unit technology. ASTM Special Technical Publication STP 1577, pp. 123 – 137.

Nasiri, E., Liu, Y. 2019. The out-of-plane behavior of concrete masonry infills bounded by reinforced concrete frames. Engineering Structures, 184, pp. 406 – 420.

Priestley, M.J.N., Elder, D.M. 1983. Stress-strain curves for unconfined and confined concrete masonry. ACI Journal Proceedings, 80(3), pp. 192 – 201, https://doi.org/10.14359/10834.

Sanchez, D.S., Feldman, L.R. 2015. Effects of transverse bar spacing on the bond of spliced reinforcing bars in concrete block masonry. ASCE Journal of Structural Engineering, 141(2), pp. 04014103 – 04014103-7.

Savkina, O.V., Feldman, L.R. 2022. Effect of concrete masonry unit web thickness on the compressive strength of concentrically and eccentrically loaded hollow masonry prisms. CSCE 2022 Annual Conference, Whistler, BC.

TMS. 2022. TMS402/602 Building code requirements and specification for masonry structures. The Masonry Society, Longmont, CO.

Vachon, T.C.J., Feldman, L.R. 2023. A reassessment of the CSA S304 chi-factor for design of reinforcing concrete masonry members: large-scale experimental investigation. Canadian Journal for Civil Engineering, 50, pp. 621 – 632. https://doi.org/10.1139/cjce-2022-0279.

Workplace Safety and Insurance Board (WSIB). 2018. Premium rates manual. https://www.wsib.ca/sites/default/files/2019-03/2018_premium_rate_manual_part_2_0.pdf, date accessed: May 29, 2019.

574 **Table 1 –** Summary of Wall Tests

Wall ID	Construction Phase	Reinf. Ratio, ρ (%)	As-Tested Prism Strength		at First Cracking		at Yielding of Reinforcement		at the Maximum Load Level	
			Ungrouted (MPa)	Corrected Grouted (MPa)	$P_{cr,total}$ (kN)	Δ_{cr} (mm)	$P_{y,total}$ (kN)	Δ_y (mm)	$P_{max,total}$ (kN)	Δ_{max} (mm)
CAD-FH-10/800-1	1	0.22	20.8	9.18	3.88	0.862	19.7	22.7	20.3	152
CAD-FH-10/800-2					4.06	1.04	19.4	23.1	20.0	152
CAD-FH-10/800-3					3.84	0.651	19.1	24.2	19.3	156
USA-FH-10/800-1			19.2	10.0	4.36	1.40	19.3	23.3	19.8	152
USA-FH-10/800-2					3.67	1.45	18.6	26.4	19.1	155
USA-FH-10/800-3					3.47	0.613	20.5	21.6	21.1	150
CAD-FH-15/800-1	2	0.44	19.8	8.54	4.48	3.08	35.2	29.8	36.1	142
CAD-FH-15/800-2					4.95	1.35	35.8	31.4	37.2	147
CAD-FH-15/800-3					4.64	-0.378	38.1	30.3	39.6	142
USA-FH-15/800-1			16.9	8.48	4.61	1.28	37.0	29.8	38.7	147
USA-FH-15/800-2					4.23	0.722	37.3	28.8	38.7	147
USA-FH-15/800-3					4.17	0.966	36.1	30.8	37.4	137
USA-KO-15/800-1	2		20.9	9.84	4.41	0.781	36.6	32.6	37.7	148
USA-KO-15/800-2					3.60	0.643	36.9	31.6	38.2	149
USA-KO-15/800-3					4.04	0.770	35.2	32.0	36.2	146
CAD-FH-20/800-1	1	0.66	20.8	10.0	1.39	0.178	48.6	31.4	50.2[2]	81.4[2]
CAD-FH-20/800-2					1.97	0.227	47.2	31.5	48.5[2]	44.5[2]
CAD-FH-20/800-3					1.45	0.649	47.2	32.5	47.9	85.3
USA-FH-20/800-1			19.2	10.6	2.95	0.736	48.2	30.7	49.3	133
USA-FH-20/800-2					2.84	0.480	46.9	31.2	48.0	86.3
USA-FH-20/800-3					4.30	0.964	48.2	34.3	49.4	141
CAD-FH-15/400-1	2	0.63	19.8	8.73	2.27	0.411	52.9	33.5	55.6	122
CAD-FH-15/400-2					7.03	-0.099	53.1	28.9	55.0	120
CAD-FH-15/400-3					6.85	0.033	53.0	31.5	55.5	128
USA-FH-15/400-1			16.9	9.54	5.54	-0.479	52.9	29.8	55.6	112
USA-FH-15/400-2					7.06	0.087	54.7	28.7	57.1	103
USA-FH-15/400-3					5.43	0.438	53.6	32.7	56.5	142

575 [2]Identified as a physical outlier at this load level.

576

577 **Table 2 –** As-Tested Properties of the Longitudinal Reinforcing Steel

Bar Size	Yield strength (MPa)	Elastic modulus (MPa)	Strain at Initiation of Strain hardening (mm/mm)	Slope at initiation of strain hardening (MPa)	Ultimate strength (MPa)	Ultimate strain (mm/mm)
10M	481	198000	0.0229	3840	602	0.140
15M	466	194000	0.0189	4190	607	0.147
20M	433	188000	0.0176	3760	567	0.170

578
579

580

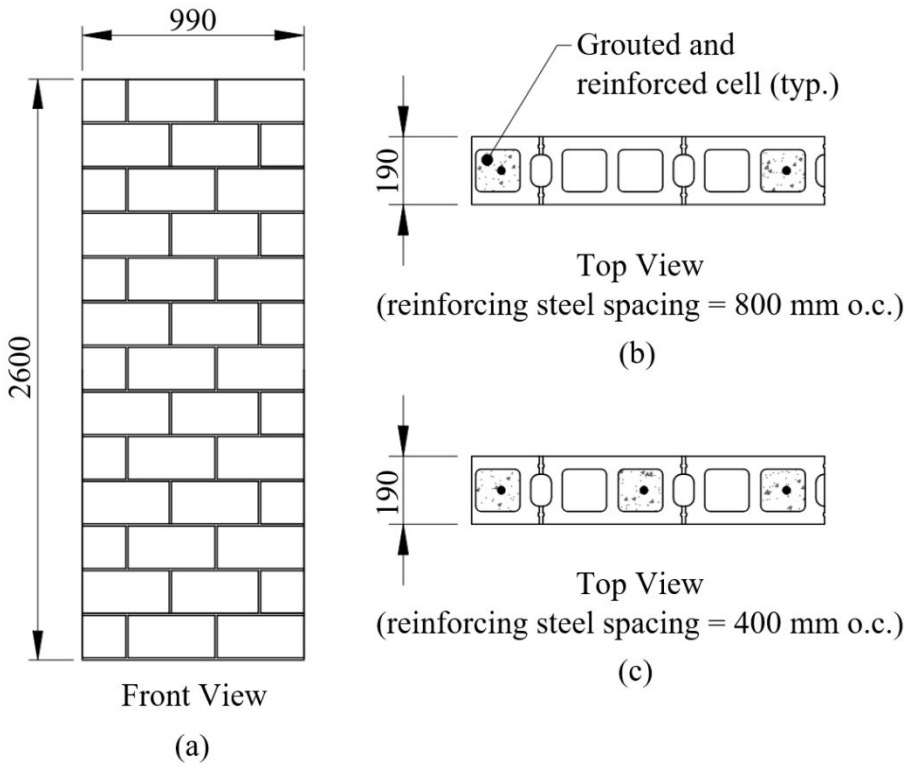

581 **Figure 1 –** Wall Details

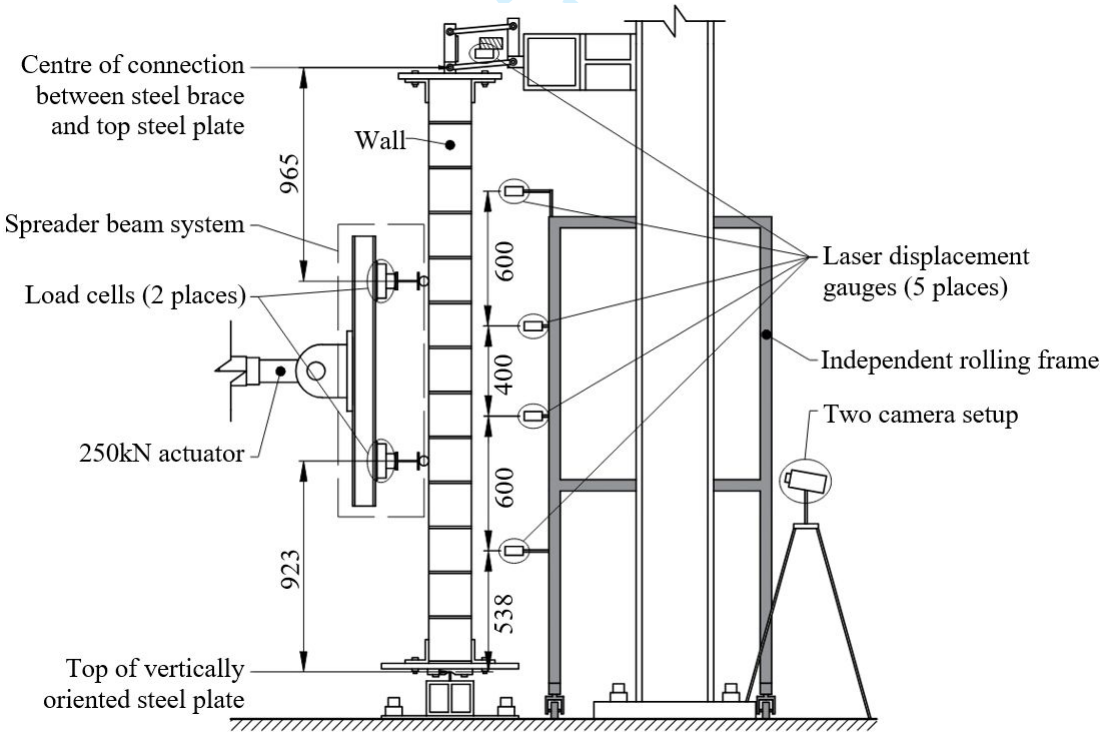

582

583 **Figure 2 –** Test setup schematic complete with instrumentation

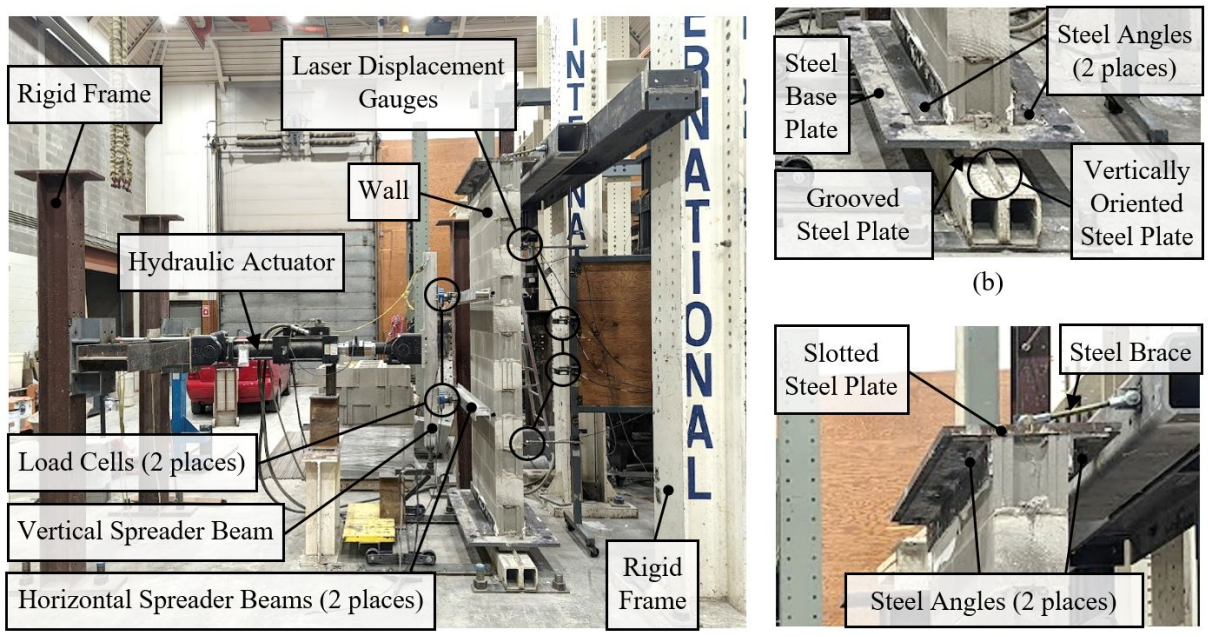

584

585 **Figure 3 –** Photograph of test setup: (a) overview, (b) bottom connection, and (c) top connection

586

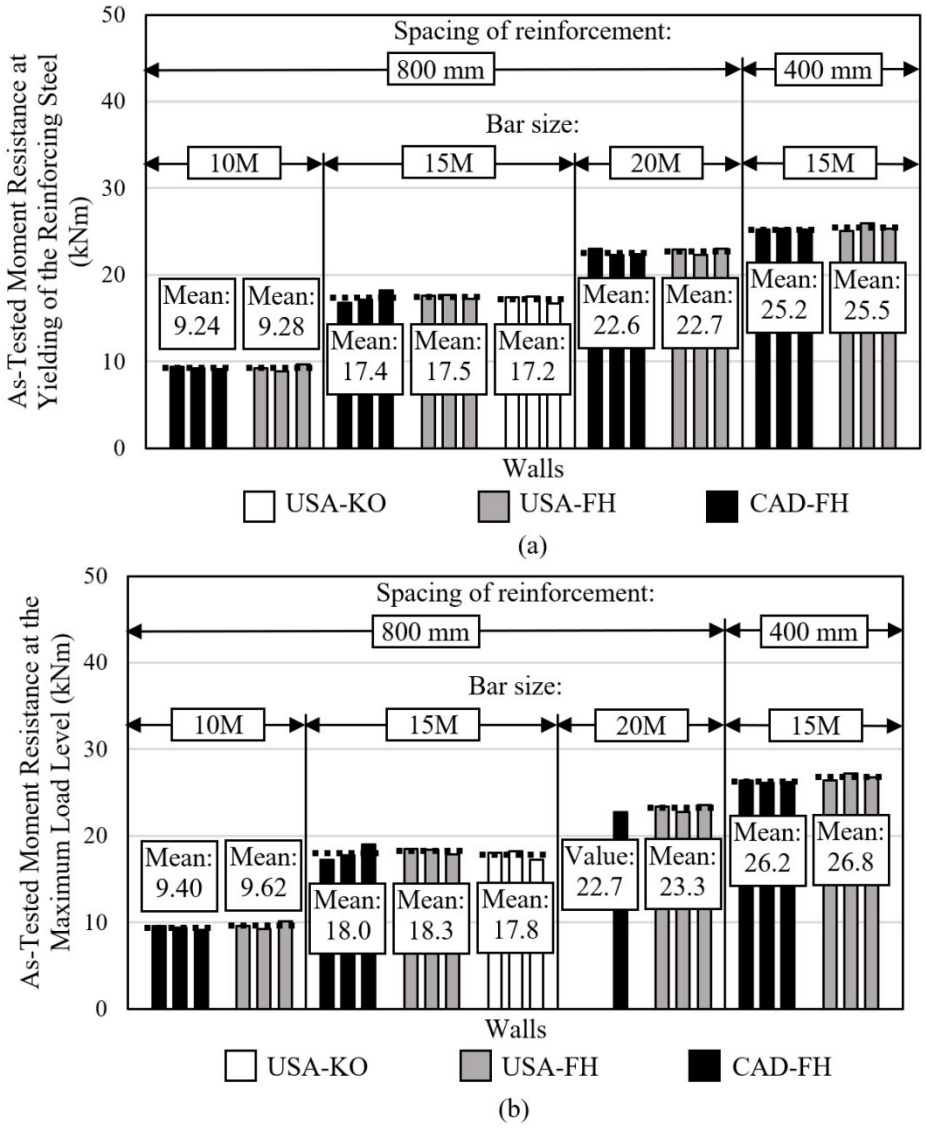

Note: Each dashed line represents the mean as-tested moment resistance for a test series.

587

588 **Figure 4 –** As-tested moment resistances: (a) at yielding of the reinforcing steel, and (b) at the

589 maximum load level.

590

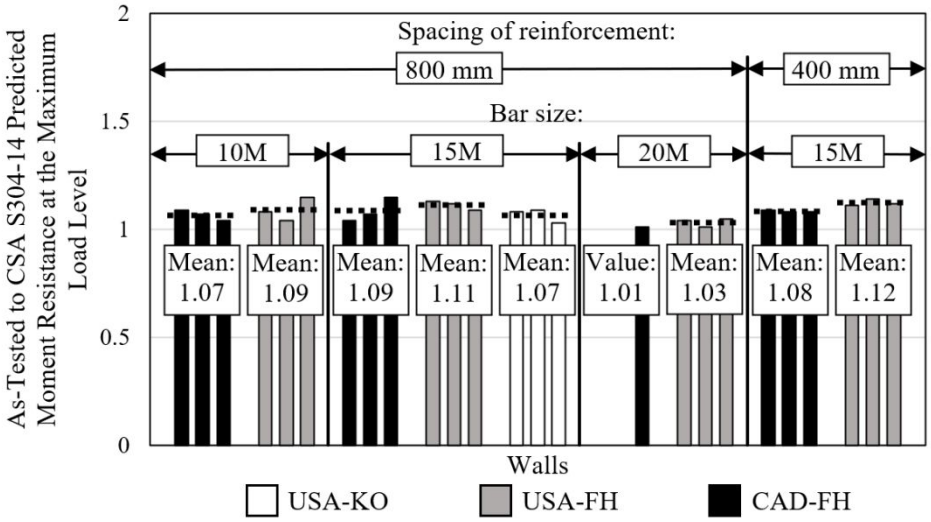

Note: Each dashed line represents the mean as-tested to CSA-S304-14 predicted moment resistance for a test series.

591 Figure 5: As-tested to CSA S304-14 predicted bending moment resistances at the maximum load

592 level.

593

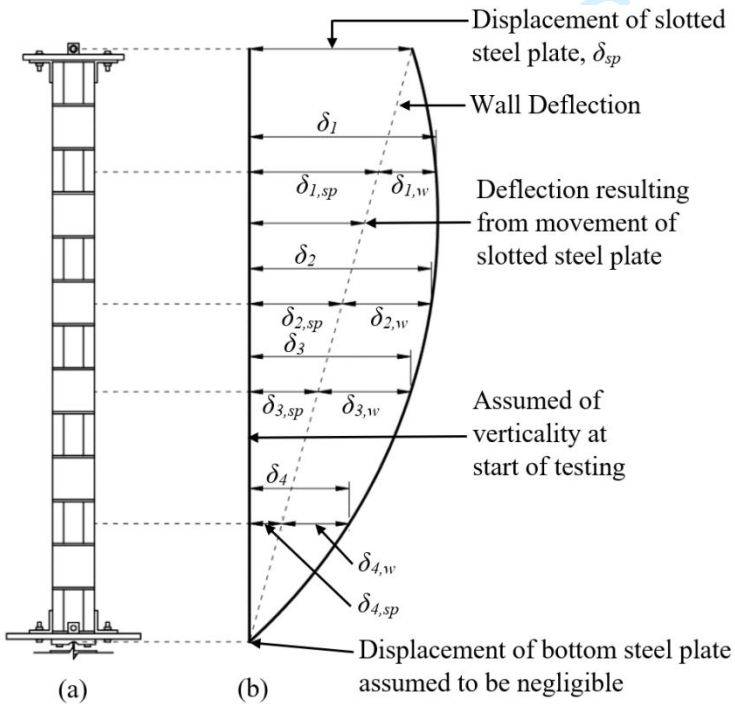

594

595 **Figure 6 –** Schematic of Wall Deflections

596

597

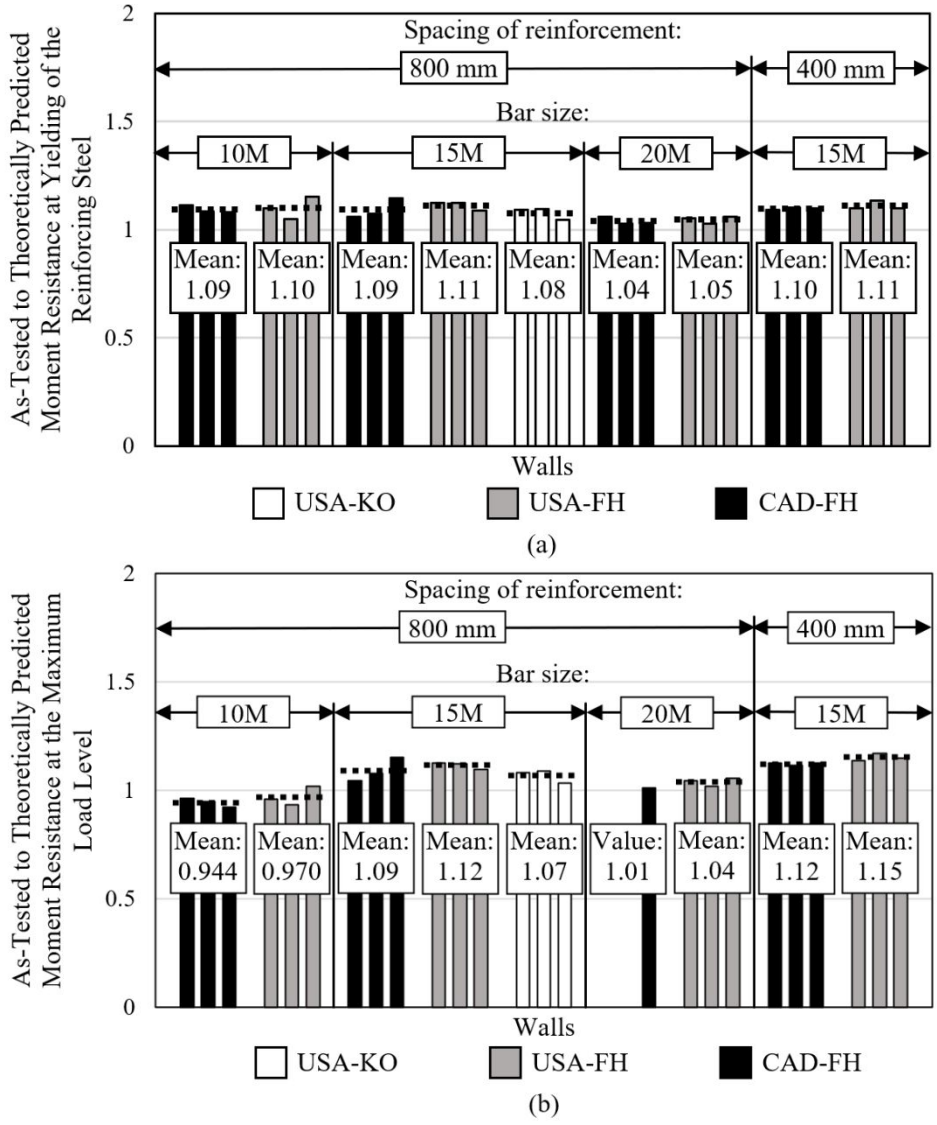

Note: Each dashed line represents the mean as-tested to theoretically predicted moment resistance for a test series.

598

599 **Figure 7 –** As-tested to theoretically predicted moment resistances: (a) at yielding of the

600 reinforcement, and (b) at the maximum load level.

601

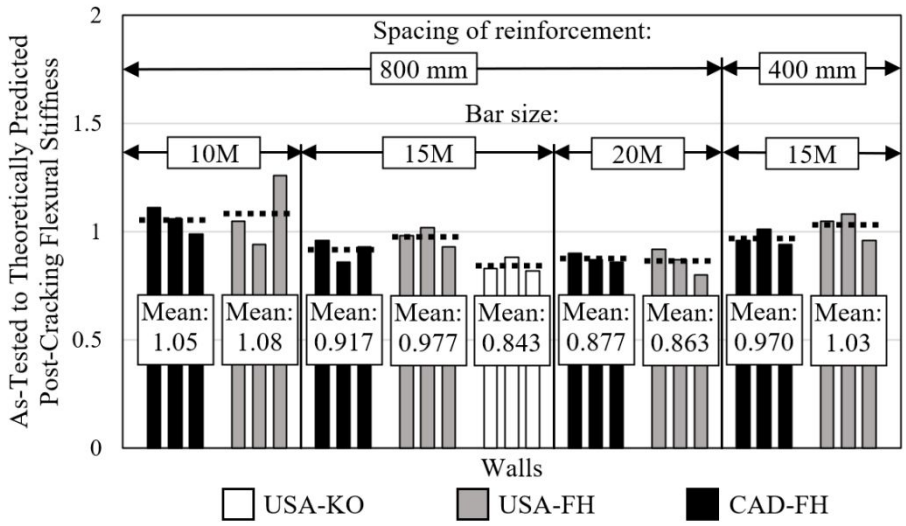

Note: Each dashed line represents the mean as-tested to theoretically predicted post-cracking flexural stiffness for a test series.

602

603 **Figure 8** – As-tested post-cracking flexural stiffness